THE ASTROPHYSICAL JOURNAL, 414:L121–L124, 1993 September 10

OBSERVATIONS OF ENTRAINMENT AND TIME VARIABILITY IN THE HH 47 JET

PATRICK HARTIGAN
Five College Astronomy Department, Graduate Research, Tower B, 517G, University of Massachusetts, Amherst, MA 01003

JON A. MORSE[1]
Department of Physics and Astronomy, University of North Carolina, CB 3255, Phillips Hall, Chapel Hill, NC 27599-3255, and Space Telescope Science Institute, 3700 San Martin Drive, Baltimore, MD 21218

STEVE HEATHCOTE
Cerro Tololo Inter-American Observatory, Casilla 603, La Serena, Chile

AND

GERALD CECIL
Department of Physics and Astronomy, University of North Carolina, CB 3255, Phillips Hall, Chapel Hill, NC 27599-3255
Received 1993 May 6; accepted 1993 June 25

ABSTRACT

We present new Fabry-Perot images of the HH 47 jet that show the first clear evidence for entrainment in a jet from a young star. The material in the jet moves faster down the axis of the flow and slower at the edges, similar to viscous flow in a pipe. The higher excitation lines occur along the edges of the jet, as expected if entrainment accelerates and heats the ambient material. We confirm previous observations of multiple bow shocks in this system. Together, time variability and entrainment produce much of the observed shock-excited gas in this object. Our data show that the "wiggles" along the jet are not caused by jet material tied to a spiraling magnetic field, but instead result from time variability, variable ejection angles, or inhomogeneities in the flow. The gas entrained in the HH 47 jet may be atomic; our results do not provide direct evidence that stellar jets drive molecular outflows.

Subject headings: ISM: kinematics and dynamics — shock waves — stars: individual (HH 46/47) — stars: pre–main-sequence

1. INTRODUCTION

Unlike most of their extragalactic counterparts, jets from young stars emit line radiation from hot regions behind shock waves in the flow. Most stellar jets can be resolved spatially from the ground, so it is possible to obtain detailed kinematic information on these flows, such as line ratios, line profiles, radial velocities and proper motions, that are impossible to measure in most other astrophysical jets. This wealth of observational data has produced a marked improvement in our understanding of the physics of highly collimated flows as well as how they affect active regions of star formation.

Schwartz (1975) first identified HH objects as shock-excited gas more than a decade ago, and HH objects were initially modeled as bow shocks around stationary cloudlets or "bullets" of dense gas ejected from the star (Schwartz 1978, 1981; Norman & Silk 1979). When HH objects were identified as the strongest shock waves of stellar jets (Dopita, Schwartz, & Evans 1982; Mundt, Brugel, & Bührke 1987) it became clear that many HH objects define the "working surfaces" of stellar jets, which have an outer bow shock that accelerates the ambient medium, and a "Mach disk" that slows the jet material (e.g., Hartigan 1989). The knots along stellar jets have proved more difficult to understand than the bow shocks, and a number of models have been proposed to explain the shocked gas in these objects, including perturbations by non-radiative cocoons (e.g., Norman et al. 1982; Norman, Smarr, & Winkler 1985), focusing cavities (Cantó, Raga, & Binette 1989), cooling (Falle, Innes, & Wilson 1987), and density gradients (Wilson & Falle 1985). However, these models cannot explain the large space motions, low shock velocities, and close knot spacings observed in stellar jets (Reipurth 1989).

Although time variability in stellar jets was first noticed by Dopita (1978), and time variability was sometimes invoked to explain the morphology of jets, the idea was first put forth in detail by Reipurth (1989) to explain observations of HH 111, HH 34, and HH 47. Time variability in stellar jets is plausible on physical grounds because disk accretion, which probably powers jets from young stars (Edwards, Ray, & Mundt 1993), varies markedly on timescales of days (Hartigan et al. 1991) to decades (Kenyon, Hartmann, & Hewett 1988). Initial analytical models of nonsteady jets by Raga & Kofmann (1992), and the more detailed one-dimensional (Hartigan & Raymond 1993) and two-dimensional (Stone & Norman 1993) numerical simulations show how shocks in stellar jets form and evolve in a variable wind. There is now clear evidence that the velocities in several flows vary dramatically—many stellar jets have multiple bow shocks which move into the wakes of previous ejections (HH 34, Reipurth & Heathcote 1992; HH 11, Solf & Böhm 1987; HH 111, Reipurth 1989; HH 47, Hartigan, Raymond, & Meaburn 1990, hereafter HRM90).

There is some observational evidence that entrainment also produces some of the observed shock structures in jets. Proper motions of the knots in the HH 34 jet recently measured by Eislöffel & Mundt (1992) are lower than expected if time variability alone causes the shock waves in the jet, and one possible explanation for these observations is that some of the knots in

[1] Visiting Astronomer, Cerro Tololo Inter-American Observatory, operated by the National Optical Astronomy Observatories under contract to the National Science Foundation.

the jet are caused by shocks that form as the jet entrains material from the surrounding medium. Solf (1987) showed that the kinematics of the HH 24C jet could be understood if the jet possessed a fast inner core surrounded by a slower envelope, and entrainment has also been invoked recently (e.g., Raga & Cabrit 1993) to explain molecular outflows. Meaburn & Dyson (1987) interpreted the range of velocities in the [S II] lines in the HH 47 jet as evidence for entrainment, but their long-slit echelle data do not clarify the spatial distribution of the emission, and they did not see extended Hα emission perpendicular to the jet.

Although entrainment is difficult to model analytically or numerically, it should have two observational characteristics. First, the average jet velocity will decrease where the flow entrains material from the ambient medium. Therefore, the highest velocity material will proceed down the axis of a jet with entrainment, with slower material confined to the edges of the flow. Second, entrainment heats the gas most in a "mixing layer" (Cantó & Raga 1991) where the velocity shear is greatest. Hence, unlike velocity variability, which produces bow shocks that have the highest excitation along the axis of the flow where the shock velocity is greatest (e.g., Stone & Norman 1993), entrainment can cause the highest excitation lines to occur away from the axis of the flow. The extent to which this latter process operates in stellar jets is unknown because entrainment has not yet been modeled in detail in two dimensions.

The recent use of Fabry-Perots to study the velocity fields in stellar jets has opened up a new dimension in this area of research. For the first time it is possible to obtain images of line emission in stellar jets at small velocity intervals. In previous papers (Morse et al. 1992, 1993a) we have used Fabry-Perot data to examine the bow shocks and Mach disks of the HH 34 and HH 111 jets. In this *Letter* we present new Fabry-Perot images of the HH 47 jet that show for the first time that entrainment produces observable shock waves in stellar jets. The new observations show that the jet moves faster along the axis of the flow and slower at the edges, with the higher excitation gas occurring at the edges of the jet. We confirm the multiple bow shocks in this flow that were found previously. Together, time variability and entrainment give rise to most, and perhaps all of the observed shock excited gas in the HH 47 system.

2. OBSERVATIONS AND REDUCTIONS

We observed the HH 47 jet in Hα and [S II] with the Rutgers/CTIO imaging Fabry-Perot on the CTIO 4 m telescope in 1991 February and 1992 January in ~1".3 FWHM seeing conditions. The TEK4 CCD provided an image scale of ~0".4 pixel^{-1} and field of view of ~2'.5 in diameter. The "narrow" etalon used has a free spectral range of 18 Å and FWHM resolution of 0.7 Å. We placed narrow-band filters in front of the etalon in order to pass a single spectral order.

We took a sequence of exposures at etalon settings which sampled the selected emission lines at regular velocity intervals, and observed the HH 46/47 system at the same velocities in each line of the [S II] doublet and Hα. The exposure times were 720 seconds for the Hα images and 600 seconds for the [S II] images. We observed the spectrophotometric standard star LTT 4364 to convert CCD counts to absolute fluxes.

Our Fabry-Perot reduction methods are discussed in detail in Morse et al. (1992, 1993a). The images were bias-subtracted and corrected for atmospheric extinction using standard IRAF routines. We then flatfielded the images and subtracted the ambient emission rings using techniques described in the above references. Finally, we phase corrected the data to produce an image of the system at each radial velocity. The reduced data consist of 17 velocity slices in Hα that span −230 to +10 km s^{-1} sampled at 15 km s^{-1} intervals, and 10 velocity slices in each line of the [S II] doublet from −230 to +40 km s^{-1} at 30 km s^{-1} intervals. These velocities are measured with respect to the globule, which has $V_{HEL} \sim +20$ km s^{-1}.

3. KINEMATICS OF THE HH 47 JET: TIME VARIABILITY AND ENTRAINMENT

The main features of the HH 47 jet are shown in the contour plot of the [S II] and Hα line emission in Figure 1, where we have followed the naming convention of Reipurth & Heathcote (1991, hereafter RH91) for the knots in the flow. The jet originates from the infrared source at the lower right of the figure, and remains highly collimated up to the bow-shaped object HH 47A. Farther along in the flow there is an extended bow shock, HH 47D; HH 47A and HH 47D were modeled by HRM90 as separate mass ejections from the infrared source. We will present shock models of the working surfaces HH 47A and HH 47D in a future paper (Morse et al. 1993b).

The velocity images of HH 47 obtained with the Fabry-Perot in Figure 2 (Plate L8) were made from the sum of the Hα and [S II] images. Figure 2 clearly shows that the fastest part of the jet is located between the infrared source and the bright bow-shaped knot HH 47A. The outer bow shock HH 47D has a much lower radial velocity than the jet, which supports the idea that HH 47A and HH 47D are separate ejections from the IRS. The emission around knot E, located near the apex of HH 47D, has a somewhat higher radial velocity than HH 47D, consistent with the idea that this region is the radiative Mach disk of the HH 47D bow shock (HRM90; RH91). Mach disks, which occur within bow shocks and mark the place where jet material is slowed, should be visible in most stellar jets (Hartigan 1989).

The HH 47 jet *splits into two separate strands* in the velocity images at −80, −110, and −140 km s^{-1}. In contrast, the fastest material (e.g., −200 km s^{-1}) appears as a single narrow jet located between the two low-velocity strands. The splitting of the jet at lower radial velocities and the location of the fastest material along the axis of the flow is exactly what should be produced by entrainment, where the fastest part of the flow is surrounded by slower material near the edges of the jet. The jet also separates into two strands in the individual Hα and [S II] velocity images as well as the sum of Hα + [S II] shown in Figure 2. The splitting of the HH 47 jet is visible in the [S II] images of RH91 (these images integrate over all velocities).

The velocity gradients in the jet are easier to see when we subtract the highest velocity images at −230, −200, and −170 km s^{-1} from the intermediate velocity images at −140, −110, and −80 km s^{-1} in Figure 3 (Plate L9). The result clearly shows that the fastest material in the jet is confined to the axis of the flow, with the slower material located at the edges of the jet. The observed kinematics are *not* consistent with a spiraling flow controlled by a magnetic field (e.g., Todo et al. 1993), because this scenario would produce alternating fast and slow radial velocities on either side of the axis of the flow. The radial velocity along the jet is not constant—the emission from knot

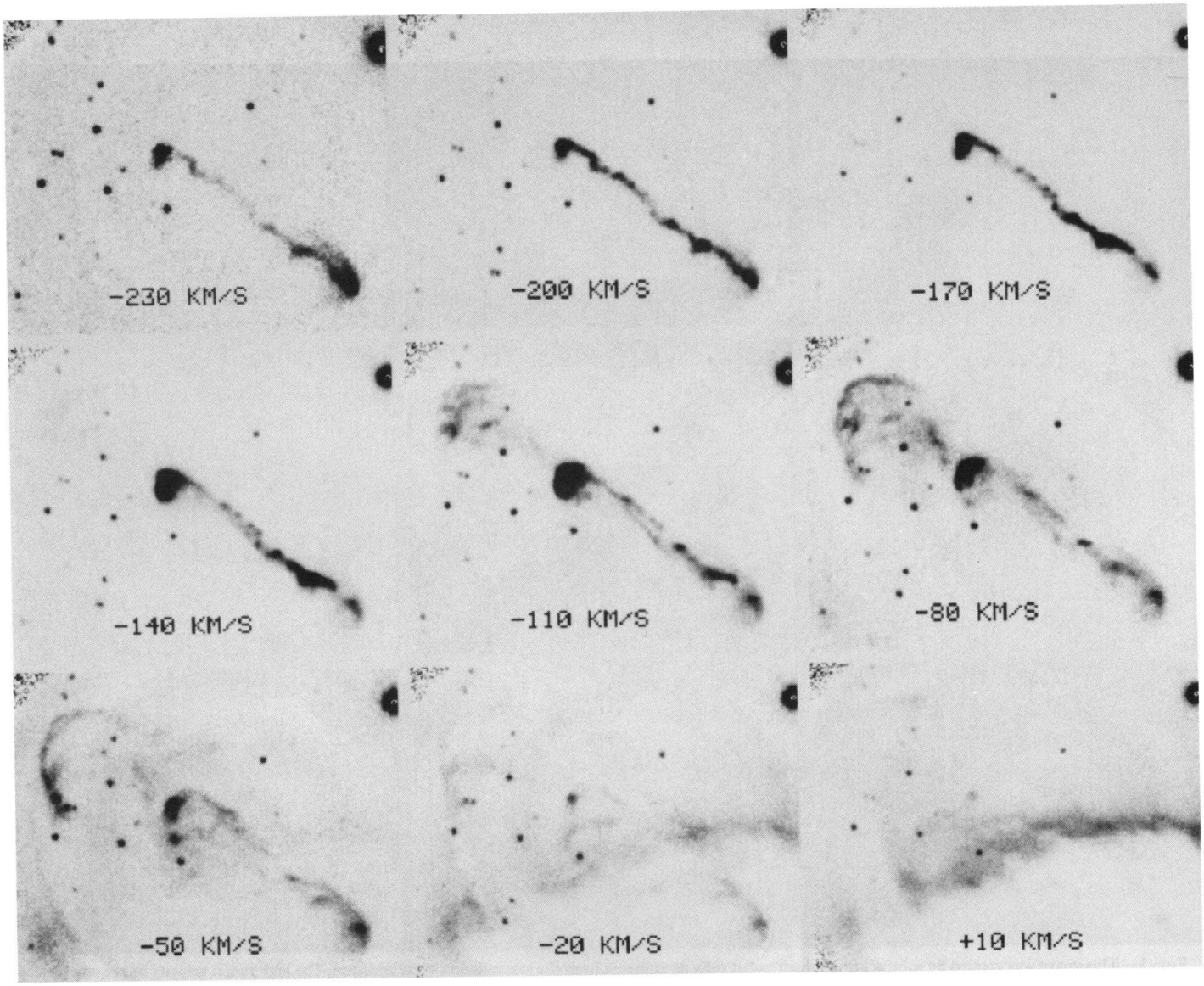

FIG. 2.—Velocity images of the HH 46/47 jet. The total [S II] and Hα emission was summed in each velocity slice to increase the signal-to-noise ratio. The radial velocities shown are with respect to the cloud velocity, which is $V_{HEL} \sim +20$ km s^{-1}. The jet splits into two strands whose separation increases at lower radial velocities. The fastest material in the jet occurs along the axis of the flow, as expected for entrainment. The outer bow shock HH 47D (see also Fig. 1) is at low radial velocities and represents a previous ejection from the young star. The faint circular artifacts in the low-velocity images are residuals in the ambient emission subtraction routine.

HARTIGAN et al. (see 414, L122)

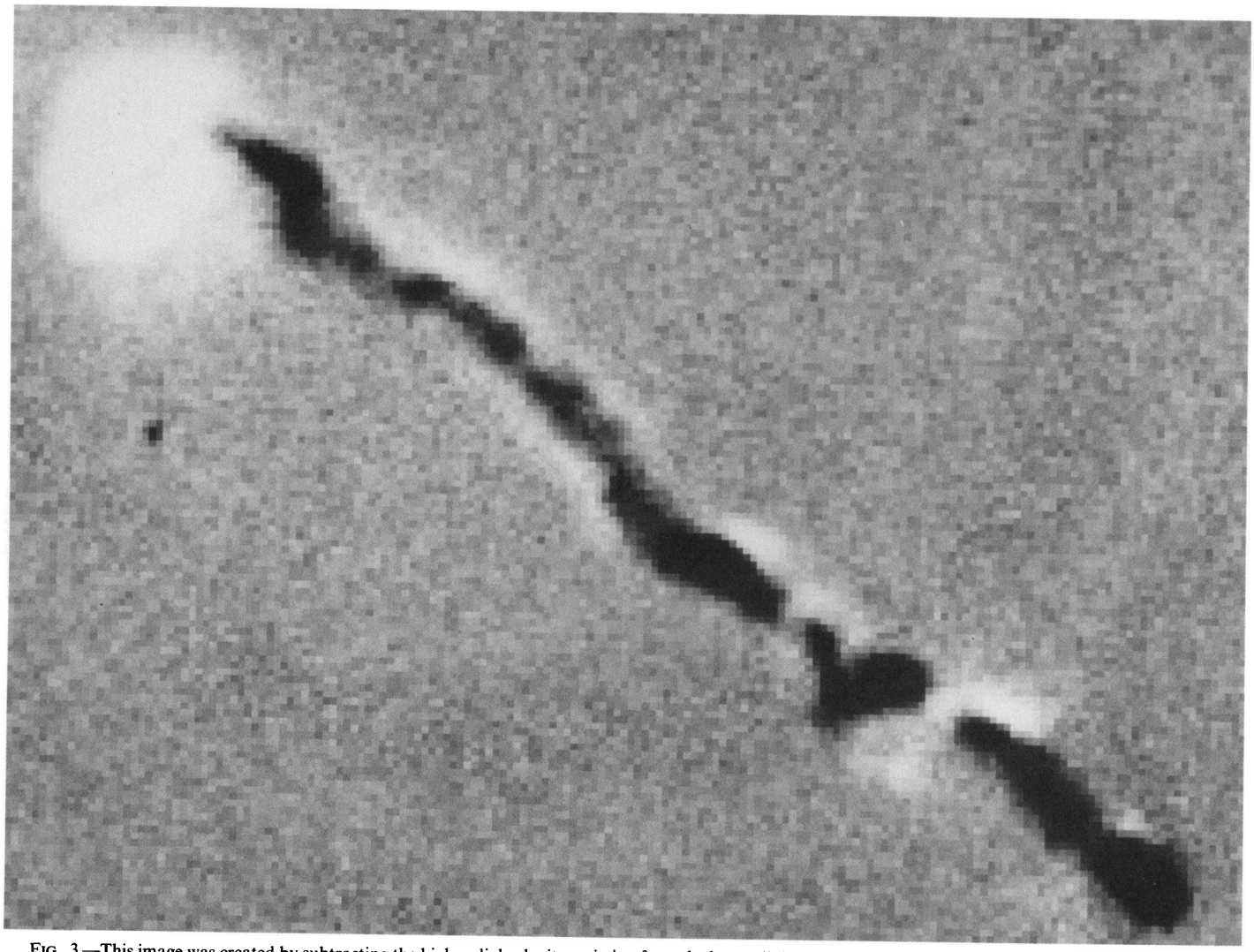

FIG. 3.—This image was created by subtracting the high radial velocity emission from the low radial velocity emission. The high radial velocity image was formed from the sum of the −230, −200, and −170 km s^{-1} images shown in Fig. 2, and the low-velocity image was made from the sum of the −140, −110, and −80 km s^{-1} images. Regions with more high-velocity emission (*black*) are surrounded by the low-velocity emission (*white*). The flow moves faster along the middle of the jet than at the edges.

HARTIGAN et al. (see 414, L122)

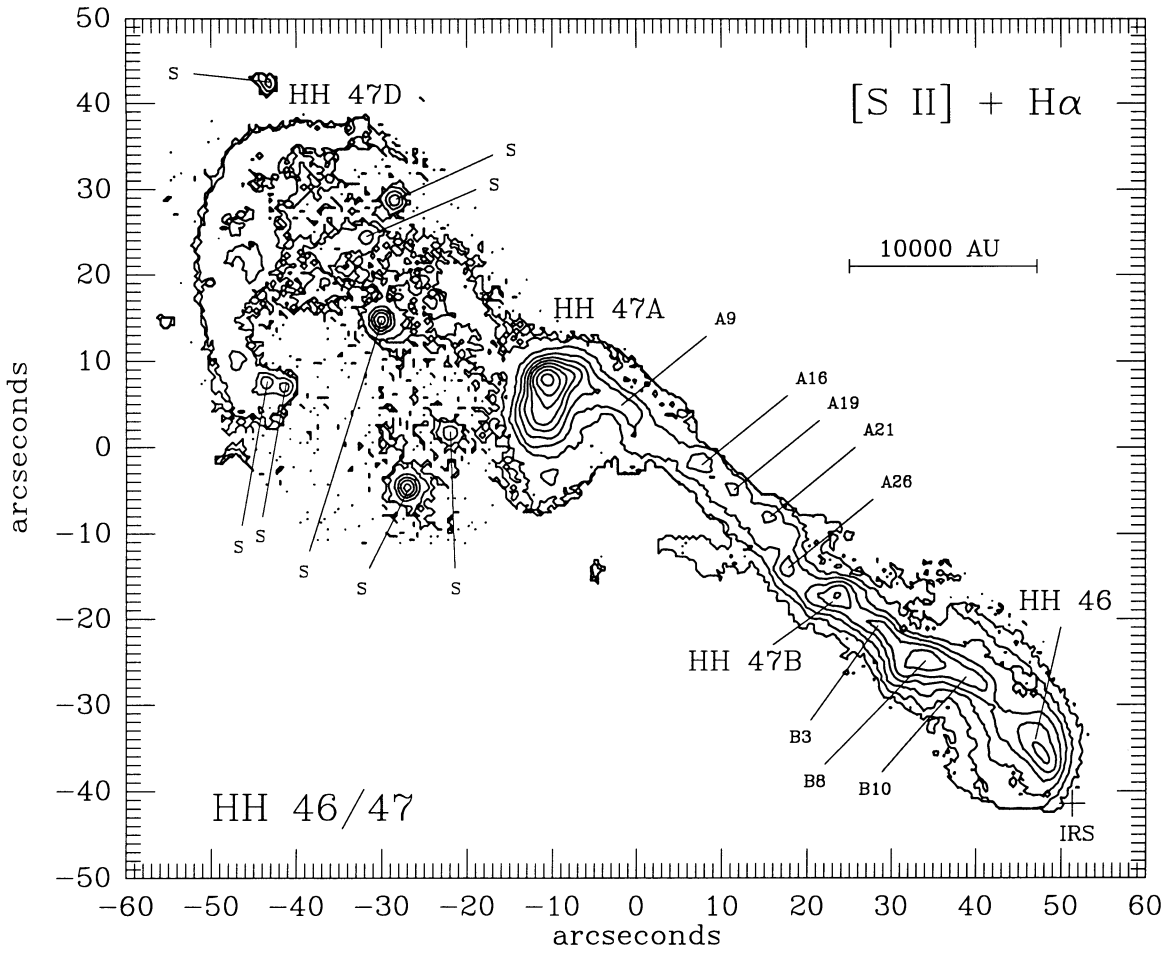

FIG. 1.—Logarithmic contour plot of the sum of [S II] λ6716, [S II] λ6731, and Hα, showing the main emission features of the HH 46/47 jet. North is to the top and east is to the left. The nomenclature of the features in the jet follows that of RH91. The infrared source that drives the jet is marked with a cross at the lower right of the figure. The scale bar shown assumes a distance of 450 pc to the object. Objects labeled "S" are stars.

B8 is ~15 km s^{-1} higher than that from knots B3 and B10 (Figures 1 and 2). These radial velocity differences could be produced by a constant radial flow whose direction varies by 2°–3° between the knots, or by a variable velocity jet.

Further evidence for entrainment is shown in Figure 4 (Plate L10), where we have subtracted the Hα images at velocities −80 to −230 km s^{-1} from the corresponding [S II] images. The subtraction image shows several interesting features, all of which are visible in the deep NTT image of RH91. There is an extended region of reflection nebulae near the IRS that is bright in Hα, and the interior of HH 47A has an Hα bright component that probably comes from the Mach disk in this object (RH91). Unlike many working surfaces of jets, HH 47A appears to be a case where the jet is less dense than the medium exterior to the bow shock, so that the Mach disk is a stronger shock than the bow shock and therefore appears relatively brighter in Hα. Figure 4 shows that the Hα emission in the jet occurs preferentially along the edges, with the central parts of the flow dominated by [S II]. Regions of the flow that have higher Hα/[S II] line ratios denote places where the shocks are strongest. The location of the hot material along the edges of the jet is consistent with entrainment.

The NTT images of RH91 have better spatial resolution than our data, but our subtraction image in Figure 4 excludes all of the low-velocity emission from the Hα rim around the globule. By comparing Figure 4 with the RH91 NTT images we can isolate the parts of the flow that are associated with the jet and observe the geometry of the shocks producing entrainment. The Hα bright knot to the south of B8, the Hα knot to the east of B8, and the Hα knot to the northwest of B are resolved by the NTT images into sharp linear features that are aligned so that they are closer to the axis of the flow at larger distances from the IRS. Indeed, all the clearly visible jet knots between positions A9 and B in Figure 1 have Hα photocenters that are displaced away from the axis of the jet and lie somewhat closer to the star than their counterparts in [S II]. If we were to model each knot as a single shock, then each shock would have to be curved so that it is more perpendicular to the flow near the edges of the jet than along the axis of the flow. New proper motion data of the knots in HH 47 from Eislöffel & Mundt (1993) indicate larger motions along the axis of the jet, consistent with our results.

4. THE JET AND THE MOLECULAR FLOW

Recently Raga & Cabrit (1993) and Stahler (1993) have suggested that molecular outflows may be entrained by stellar jets.

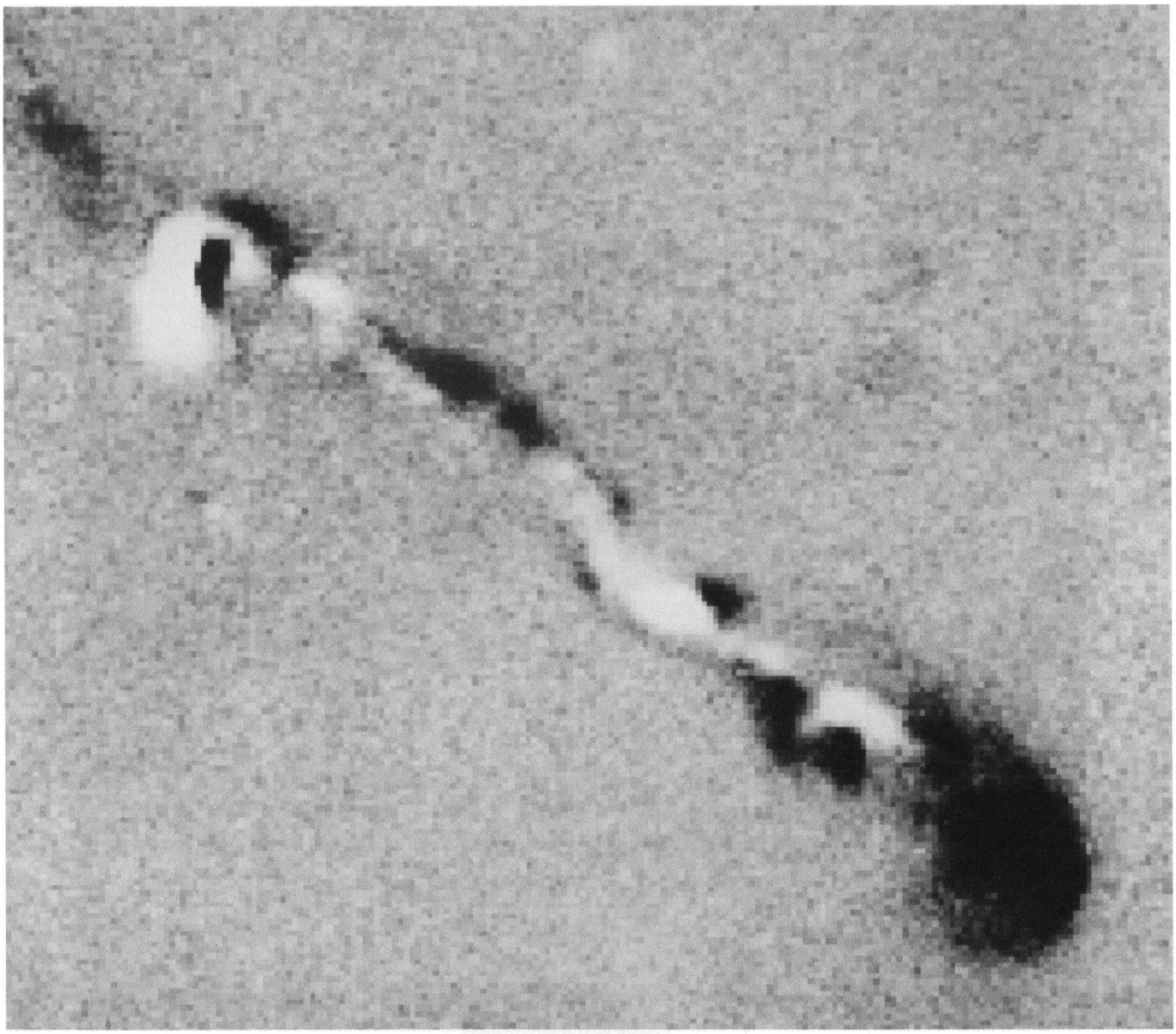

FIG. 4.—Difference image of [S II] minus Hα made using the velocity images from −80 to −230 km s^{-1}. Regions stronger in Hα are black, and those stronger in [S II] are white. The seeing is worse than in a similar image in RH91, but we are able to exclude the bright ambient emission at low velocities that obscures much of the structure between HH 47B and HH 47A in the RH91 image. The material at the outer edges of the jet tends to be brighter in Hα.

HARTIGAN et al. (see 414, L123)

The molecular outflow mapped by Chernin & Masson (1991) has also been explained in terms of entrainment. Our Fabry-Perot observations do not rule out the idea that jets drive outflows by entrainment, but the present observations do not necessarily support this model either. In the Raga & Cabrit (1993) model most of the entrainment occurs in the wake of the bow shock, which in this case should be directly behind HH 47A. However, we observe entrainment equally along the entire length of the jet. The jet remains highly collimated all the way from the IRS to HH 47A, and does not dissipate as it entrains material, as suggested recently (Stahler 1993).

The outer bow shock HH 47D extends all the way back to near the IRS in the [O II] images of HRM90. Hence, the gas within HH 47D, including the material now being entrained at the edges of the jet, either passed through HH 47D earlier in the history of the flow or was originally jet gas that was decelerated and channeled out of the Mach disk of HH 47A at an earlier time when 47A was much closer to the exciting source. In either case, the gas within this cavity is likely to be mostly atomic rather than molecular because the material has passed through a relatively high-velocity shock earlier in the lifetime of the flow. Surprisingly, molecular hydrogen emission has been identified in HH 47A by Böhm, Scott, & Solf (1991) with *IUE*, so molecules must either reform out of postshock atomic gas or survive the shock waves in this object. Deep H_2 images of this system would help to clarify whether or not the optical jet interacts with the molecular flow. The *K* band image of Graham & Heyer (1989) does not show any evidence for H_2 emission along the jet.

The numerical simulations of Stone & Norman (1993) show how the passage of bow shocks opens up a cavity like that outlined by HH 47D, and the molecular outflow may occur along the edges of this cavity. However, the physics of the acceleration of molecular gas by the wings of bow shocks probably involves C shocks or magnetic precursors, and has not yet been modeled in detail.

We thank John Raymond for his comments on a draft of this paper, and an anonymous referee for his/her suggestions. We also thank the CTIO staff, especially Bob Schommer, for their expert assistance with the instrumentation. P. H. was supported by NSF grant 91A1042 to S. Strom and the NASA Planetary Program during the course of this work. Research on high-velocity gas flows by J. M. and G. C. is supported by the NSF. J. A. M. was also supported by NASA grants NAGW-2689 and NAGW-3268 at STScI.

REFERENCES

Böhm, K.-H., Scott, D. M., & Solf, J. 1991, ApJ, 371, 248
Cantó, J., & Raga, A. 1991, ApJ, 327, 646
Cantó, J., Raga, A., & Binette, L. 1989, Rev. Mexicana Astron. Af., 17, 65
Chernin, L. M., & Masson, C. R. 1991, ApJ, 382, L93
Dopita, A. 1978, A&A, 63, 237
Dopita, M., Schwartz, R. D., & Evans, I. 1982, ApJ, 263, L73
Edwards, S., Ray, T., & Mundt, R. 1993, in Protostars and Planets III, ed. E. Levy & J. Lunine (Tucson: Univ. Arizona Press), 567
Eislöffel, J., & Mundt, R. 1992, A&A, 263, 292
———. 1993, in preparation
Falle, S., Innes, D., & Wilson, M. 1987, MNRAS, 225, 741
Graham, J. A., & Heyer, M. 1989, PASP, 101, 573
Hartigan, P. 1989, ApJ, 339, 987
Hartigan, P., Kenyon, S., Hartmann, L., Strom, S., Edwards, S., Welty, A., & Stauffer, J. 1991, ApJ, 382, 617
Hartigan, P., & Raymond, J. 1993, ApJ, 409, 705
Hartigan, P., Raymond, J. C., & Meaburn, J. 1990, ApJ, 362, 624 (HRM90)
Kenyon, S., Hartmann, L., & Hewett, R. 1988, ApJ, 325, 231
Meaburn, J., & Dyson, J. E. 1987, MNRAS, 225, 863
Morse, J. A., Hartigan, P., Cecil, G., Raymond, J. C., & Heathcote, S. 1992, ApJ, 399, 231
Morse, J. A., Hartigan, P., Heathcote, S., Raymond, J. C., & Cecil, G. 1993b, in preparation
Morse, J. A., Heathcote, S., Cecil, G., Hartigan, P., & Raymond, J. C. 1993a, ApJ, June 20, in press
Mundt, R., Brugel, E. W., & Bührke, T. 1987, ApJ, 319, 275
Norman, C. A., & Silk, J. 1979, ApJ, 228, 197
Norman, M. L., Smarr, L., Winkler, K.-H., & Smith, M. D. 1982, A&A, 113, 285
Norman, M. L., Smarr, L., & Winkler, K.-H. 1985, in Numerical Astrophysics, ed. J. Centrella, J. LeBlanc, & R. Bowers (Boston: Jones and Bartlett), 88
Raga, A., & Cabrit, S. 1993, A&A, in press
Raga, A. C., & Kofman, L. 1992, ApJ, 386, 222
Reipurth, B. 1989, in Low-Mass Star Formation and Pre–Main-Sequence Objets, ed. B. Reipurth (Garching: ESO), 247
Reipurth, B., & Heathcote, S. R. 1991, A&A, 246, 511 (RH91)
———. 1992, A&A, 257, 693
Schwartz, R. D. 1975, ApJ, 195, 631
———. 1978, ApJ, 223, 884
———. 1981, ApJ, 243, 197
Solf, J., & Böhm, K.-H. 1987, AJ, 93, 1172
Stahler, S. 1993, in Astrophysical Jets, ed. M. Livio, C. O'Dea, & D. Burgarella (Cambridge: Cambridge Univ. Press), in press
Stone, J., & Norman, M. 1993, ApJ, 413, 198
Todo, Y., Uchida, Y., Sato, T., & Rosner, R. 1993, ApJ, 403, 164
Wilson, M. J., & Falle, S. 1985, MNRAS, 216, 971

Note added in proof.—Zealey, Suters, & Randall (Proc. Astron. Soc. Australia, in press [1993]) have discovered molecular hydrogen emission along the edges of the outflow cavity in HH 47 and also along the jet.